Published in final edited form as:
J Phys Chem B. 2013 August 8; 117(31): . doi:10.1021/jp401551t.

Distance-Independent Charge Recombination Kinetics in Cytochrome *c* - Cytochrome *c* Peroxidase Complexes: Compensating Changes in the Electronic Coupling and Reorganization Energies

Nan Jiang[a], **Aleksey Kuznetsov**[a], **Judith M. Nocek**[b], **Brian M. Hoffman**[b], **Brian R. Crane**[c], **Xiangqian Hu**[a,*], and **David N. Beratan**[a,d,e,*]

[a]Department of Chemistry, Duke University, Durham, NC 27708

[b]Department of Chemistry, Northwestern University, Evanston, IL 60208

[c]Department of Chemistry and Chemical Biology, Cornell University, Ithaca, NY 14853

[d]Department of Biochemistry, Duke University, Durham, NC 27708

[e]Department of Physics, Duke University, Durham, NC 27708

Abstract

Charge recombination rate constants vary no more than three-fold for inter-protein ET in the Zn-substituted wild type (WT) cytochrome *c* peroxidase (CcP):cytochrome *c* (Cc) complex and in complexes with four mutants of the Cc protein (i.e., F82S, F82W, F82Y and F82I), despite large differences in the ET distance. Theoretical analysis indicates that charge recombination for all complexes involves a combination of tunneling and hopping via Trp191. For three of the five structures (WT and F82S(W)), the protein favors hopping more than that in the other two structures that have longer heme→ZnP distances (F82Y(I)). Experimentally observed biexponential ET kinetics is explained by the complex locking in alternative coupling pathways, where the acceptor hole state is either primarily localized on ZnP (slow phase) or on Trp191 (fast phase). The large conformational differences between the CcP:Cc interface for the F82Y(I) mutants compared to the WT and F82S(W) complexes are predicted to change the reorganization energies for the CcP:Cc ET reactions because of changes in solvent exposure and inter-protein ET distances. Since the recombination reaction is likely to occur in the inverted Marcus regime, an increased reorganization energy compensates the decreased role for hopping recombination (and the longer transfer distance) in the F82Y(I) mutants. Taken together, coupling pathway and reorganization energy effects for the five protein complexes explains the observed insensitivity of recombination kinetics to donor-acceptor distance and docking pose and also reveals how hopping through aromatic residues can accelerate long-range ET.

Keywords

electron transfer; cytochrome *c* oxidase; cytochrome *c*; tunneling; hopping; tunneling pathways

[*]xqhu@duke.edu; Tel: (919) 218-7779, david.beratan@duke.edu; Tel: (919) 660-1526.

ASSOCIATED CONTENT

SUPPORTING INFORMATION AVAILABLE:

Figures S1–S7, Tables S1–S6, and complete refs 83, 90 and 108. This material is available free of charge via the Internet at http://pubs.acs.org.

Introduction

Electron-transfer (ET) reactions across protein-protein interfaces underlie the flow of energy in all biological systems.[1–6] Nonetheless, interprotein ET is less well understood than intraprotein ET due to complications that arise from the long distances, the complex medium separating the donor (D) and acceptor (A), and the association reactions of the interacting partners.[1–8] Within these protein assemblies, ET reactivity depends on many interdependent factors that include the juxtaposition of redox sites, the bonding networks connecting D/A, the conformational dynamics coupled to molecular recognition, the electrochemical potentials, and the reorganization energies. It is perhaps not surprising that both protein-protein recognition and ET are strongly influenced by residue substitutions, which thereby offer the means to probe the effects of specific structural perturbations on these complex processes.[5,9–23] In this study we examine how the association of a protein-protein complex influences the kinetics and mechanism of biological ET.

The cytochrome *c* peroxidase (CcP) - yeast cytochrome *c* (yCc) couple (i.e., wild type (WT) CcP:yCc or CcP:Cc, shown in Figure 1) has served as a paradigm to explore how changes to the inter-protein interface influence ET rates.[11,24,25,26] Hoffman and coworkers studied the photo-initiated ET cycle shown in Figure 2 for Zn-porphyrin (ZnP) substituted CcP (ZnCcP). ZnP is photo-excited and relaxes to its triplet excited state (^{3}ZnP) on the ns time scale, and ET occurs from ^{3}ZnP to Fe^{3+}Cc. The charge-separated species produced, [Zn(II)CcP$^{\bullet+}$, Fe(II)Cc], returns to the ground state by back ET, i.e., Fe(II)Cc → Zn(II)CcP$^{\bullet+}$. The back reaction can be considered as a photo-triggered analogue for the physiological ET reaction between Fe(II)Cc and Compound I. Both involve a radical species at Trp191 (*vide infra*) and Compound I likely has a similar potential to Zn(II)CcP$^{\bullet+}$ (1.20 V vs. 0.9–1.15 V, respectively.[27] Experimental studies[9,18–27] indicate that the back ET rate (i.e., the dominant fast phase of the kinetics found in both solution phase and crystalline protein-protein complex ET) from yeast Cc to CcP is insensitive to conformational and distance changes that are caused by single-residue mutations in Cc (i.e., in F82W, F82S, F82Y, and F82I). This theoretical study examines the molecular mechanism of the charge recombination in all five complexes and probes the origins of the similarity in the recombination rates of WT, F82S(W), and F82Y(I) (note that Cc and CcP are dropped here for brevity).

The crystal structures of Crane and coworkers indicate that the Cc F82S(W) mutants maintain the same relative conformations between the CcP and the Cc as in the WT CcP:Cc complex. Highly conserved Cc residue F82 resides at the heme edge and buries 13 Å^2 of solvent accessible surface area in the interface with CcP.[9] As shown in Figures 1 and S1 of the Supporting Information (SI), after aligning the CcP units of all five protein complexes, the F82S(W) complexes do not show large structural changes compared to the WT CcP:Cc structure (although greater conformational variability was noted at the interface in the mutants compared to WT.[9] In contrast, the Cc F82Y(I) variants show a dramatic change in complex assembly in which the Cc units are rotated by roughly 90 degrees with respect to the aligned CcP unit (see Figure S1). In these altered association modes, Y(I)82 no longer participates in the interface with CcP. These changes in the protein-protein interfaces increase the donor (D) to acceptor (A) distance ($\boldsymbol{R_{DA}}$) for F82Y(I) by 3–7 Å, measured either edge-to-edge or metal-to-metal, compared to WT CcP:Cc and to F82S(W) (see Figure 3). Consequently, F82Y(I) mutants are expected to have ET rates two orders of magnitude slower than in the WT CcP:Cc and F82S(W) complexes based on square barrier tunneling models[28–30] with $\boldsymbol{k_{ET} \propto \exp[-\beta R_{DA}]}$ and β = 1.1 Å^{-1}. Surprisingly, the measured back ET rate constants for fast kinetic phase in the WT and all four mutant complexes, both in crystals and in solution, are the same order of magnitude[9,18,31] (k_{eb} = 6,000 s^{-1} for WT, 5,800 s^{-1} for F82W, 2,000 s^{-1} for F82S, 2,100 s^{-1} for F82I, and 4,000 s^{-1} for F82Y in the

crystals, see Table 1 for experimental rates measured both in crystals by Crane and coworkers[9,31] and in solution by Hoff-man and coworkers.[18] Likewise, the rate constants for the slower of the phases observed in both crystals and in solution (k = 10–100 s^{-1}, Table 4) are similar in magnitude for all of the mutants.[30] In this manuscript, we aim to understand why the increased donor-acceptor distances associated with Cc rotation by 90 degrees in the F82Y(I) complexes does not dramatically slow down the ET recombination rates for either kinetic phase compared with rates in the WT CcP:Cc and F82S(W) complexes.

Experimental studies indicate that multistep electron recombination via an aromatic amino acid (such as tryptophan) is essential for long-range ET in many biological systems that include photolyases and cryptochromes,[32] photosynthetic reaction centers,[33] nitric-oxide synthases,[34] and perhaps most significantly, between the R1 and R2 subunits of ribonucleotide reductase.[35,36] The CcP:Cc system is an excellent model for understanding the parameters that govern such electron "hopping" reactions.[9,11,18,21,31,37–39] In fact, Hoffman *et al.*[40] suggested that the fast step of the charge recombination ET in CcP:Cc involves hopping through the tryptophan radical cation, $W191^{+\bullet}$ (Figure 2), which is 3.6 Å away (edge-to-edge) from ZnP, as shown in Figure 3, and Crane *et al.*[9,31] suggested a rapid equilibrium between the Zn-porphyrin radical cation and the tryptophan radical. As such, hopping through Trp191 may enhance the back ET rates in both the WT CcP:Cc and mutant complexes. Indeed, in metal-modified proteins, Gray and coworkers showed that tryptophan centered ET intermediates can enhance ET rates between distant Cu and Re species (in *Pseudomonas aeruginosa* azurin) by two orders of magnitude compared to the single-step mechanism.[38,39,41] Here, we examine the proposed CcP:Cc hopping mechanism in detail and systematically explore whether the source of the observed rate compression lies in effects of (1) tunneling pathways coupling, (2) reorganization energy, (3) or hole hopping through W191.

The high-temperature non-adiabatic ET rate is[1]

$$k_{ET} = \frac{2\pi}{\hbar} \frac{\langle H_{DA}^2 \rangle}{\sqrt{4\pi\lambda k_B T}} exp\left[-\frac{(\Delta G + \lambda)^2}{4\lambda k_B T} \right] \quad (1)$$

where $\langle H_{DA}^2 \rangle$ is the ensemble averaged square of the protein-mediated donor-acceptor electronic coupling, λ is the reorganization energy, ΔG is the reaction free energy, k_B is Boltzmann' s constant, and T is the temperature (298 K). Inter-protein electronic couplings can be approximated using semi-empirical electronic structure theory on protein geometries sampled with classical molecular dynamics (MD). These computational schemes were applied in the past to small organic molecules, proteins, and nucleic acids.[11,42–66] In this study, the mean-squared coupling, $\langle H_{DA}^2 \rangle$, was first computed using PATHWAY analysis[67] of MD snapshots to examine relative couplings. The key residues that mediate electron tunneling are readily identified in the PATHWAY analysis. Subsequent semi-empirical quantum mechanical analyses (i.e., INDO[68]), in combination with two-state generalized Mulliken-Hush calculations of couplings[69,70] (i.e., INDO-GMH), were used to characterize the molecular orbitals involved in the ET recombination and to estimate mean-squared couplings. Eq. 1 can overestimate the drop off of the ET rate when - $\Delta G > \lambda$ (the inverted regime)[71] because it does not include corrections from quantized vibrational modes coupled to ET. Such quantum correction to the ET rate can be particularly important in smaller organic molecules containing spatially localized donor or acceptor groups with high frequency vibrational modes.[1,71] However, studies of ΔG-dependent rates in modified proteins and model systems display a wide range of behaviors in the inverted regime, depending upon molecular structure.[72–74] As such, it is difficult to predict the quantitative extent of rate slowing in the inverted region, even given an accurate value for the outer

sphere reorganization energy. Thus, we use the simple high temperature (classical) form for the ET rate expression with a simple (continuum) model for λ.

Our studies indicate that a hopping recombination mechanism through Trp191 for all five protein complexes contributes to the ET recombination rates (10% of snapshots for WT and F82S(W) and less than 1% of snapshots for F82Y(I)), in addition to direct heme-ZnP tunneling.[40] To interpret the unusually weak distance dependence for the back ET rate, we also computed the approximate outer sphere reorganization energies for the WT CcP:Cc complex and the four mutants, using two qualitative schemes, the Marcus two-sphere model[71] and the finite-difference Poisson-Boltzmann approach.[75] The crystallographically characterized CcP:Cc complexes offer a unique opportunity to investigate how ET reactions involving the same donor and acceptor sites embedded in the same protein matrices can be influenced by changes in reorganization energy due to different geometries and solvation environments. As expected, we find that the reorganization energy grows with the D-A distance, and that this dependence compensates for decreased electronic couplings in the F82Y(I) mutants. The charge recombination ET is "inverted" in these proteins, so the recombination rate accelerates as λ grows. Taken together, the compensating decrease of coupling with distance and the growth of λ with distance explain the observation of similar back ET rate constants in the WT and mutant protein-protein complexes, despite the fact that the heme-ZnP distances differ by 3–7 Å among the complexes; the distance range would, itself, be expected to induce a variation of $10^2 - 10^4$ -fold in rate constants.

Computational Details

A. Modeling protein structures and fluctuations

The initial structures for MD simulations of the WT ZnCcP:Cc complex and its four mutants were taken from the crystal structures of the CcP:Cc complexes (PDB IDs are 1U74[31], 2B10[9] , 2B11[9] , 2B0Z[9], and 2B12[9], respectively). Hydrogen atoms were added using VMD.[76] In all simulations, the NAMD 2.6b1 program[77] was used with the CHARMM27 force field.[78–80] Constant pressure MD simulations were performed (NPT ensemble, 1 atm, 298 K) with a Langevin thermostat, periodic boundary conditions, and particle mesh Ewald electrostatics to take the long-range electrostatic interactions into account. Since the measured back ET rate constants in solution are similar to those found in the CcP:Cc crystals, we carried out MD simulations in aqueous solution using the docked crystal structures.[9] For WT CcP:Cc, the structure was solvated in a TIP3P water box of 105 × 90 × 75 $Å^3$ with 20,940 water molecules, including 183 crystallographic water molecules. The total number of atoms in the WT CcP:Cc structure was 69,287. After an initial 5,000 step energy minimization, a 300 ps MD simulation was carried out at 298 K while constraining the entire protein geometry but allowing waters to move. Then, an unconstrained 500 ps MD simulation was performed at 298 K to equilibrate the system. Finally, a 10 ns MD simulation was carried out, and conformations were saved every 2 ps. This procedure was used to prepare the starting structures for the other four protein complexes. Overall, 5,000 snapshots were saved for each protein complex over 10 ns of simulation, and the last 2,000 snapshots were used to compute the coupling elements.

B. PATHWAY model

The pathways plugin for VMD[67,81] was used to compute the relative couplings for each MD snapshot. The PATHWAY model[67] is

$$H_{DA} \propto \prod_i \varepsilon_i^C \prod_j \varepsilon_j^H \prod_k \varepsilon_k^S \quad (2)$$

where Π represents a product. The penalty for tunneling through a covalent bond is $\boldsymbol{\varepsilon^c = 0.6}$, the penalty for a through-space jump is $\boldsymbol{\varepsilon^s = (\varepsilon^c)^2 exp[-1.7(R^s - 1.4)]}$, where $\boldsymbol{R^s}$ is the through-space distance in Å, and the penalty for a hydrogen bond-mediated step is $\boldsymbol{\varepsilon^H = \varepsilon^c exp[-1.7(R^H - 2.8)]}$, where $\boldsymbol{R^H}$ is the hydrogen bond length (heavy atom to heavy atom) in Å. The mean-squared donor-acceptor electronic coupling enters the ET rate constant[8] as $\boldsymbol{k_{ET} \propto \langle H_{DA}^2 \rangle}$. (In addition, we calculated ET couplings using a "softer" through-space decay exponent of $\beta = 1.1$ Å^{-1} instead of a through-space decay exponent of $\beta = 1.7$ Å^{-1} in the $\boldsymbol{\varepsilon^s}$ and $\boldsymbol{\varepsilon^H}$ terms.[46,56] We found similar trends, leading to the same conclusions). In the PATHWAY analysis, Zn and all heavy atoms on the aromatic porphyrin ring were defined as members of the acceptor group in CcP, while only the Fe atom in the Cc heme was chosen as the donor.[82]

C. Computing electronic couplings with INDO-GMH

Semi-empirical quantum mechanics (QM), i.e., INDO with two-state GMH analysis of couplings, was used to calculate $\boldsymbol{\langle H_{DA}^2 \rangle}$ using protein-protein complex snapshots and to characterize electron mediation by the proteins. The key residues included in the INDO calculations were identified using PATHWAY analysis for each MD snapshot. Among the 2,000 snapshots for each protein complex, the frequency of residues appearing in the strongest ET pathways was first determined. Residues that appeared more than 500 times (as well as water molecules within a 5 Å cutoff radius around Ala194 of CcP) were included in the INDO calculations. (Since only the residues near Ala194 of CcP are exposed to bulk water, we studied the dependence of $\boldsymbol{\langle H_{DA}^2 \rangle}$ on the cutoff radius for water molecules included in the QM calculations. The $\boldsymbol{\langle H_{DA}^2 \rangle}$ values changed by less than 5% as the radius grew from 5 Å to 10 Å around Ala194 of CcP.) For example, the residues included in the INDO calculations of the WT CcP:Cc complex are labeled in Figure 4. The amino acids and functional groups included in the INDO computations for the WT Cc:CcP complex and for the mutants are shown in Table S1. Typically, the INDO calculations contained 320–370 atoms from protein and solvent.

On the porphyrins, Fe has five valence d orbitals and ZnP has three valence p orbitals. If Trp191 is an ET intermediate, its high lying filled frontier orbitals would participate in recombination ET. Therefore, the frontier molecular orbitals (MOs) from HOMO to HOMO-10 were computed with the INDO method for each of the 2,000 protein snapshots for the five protein complexes. These orbitals were identified as donor and acceptor orbital pairs[51,53,83] for the Fe(II)Cc → Zn(II)CcP$^{\bullet+}$ ET reaction. Ten frontier occupied molecular orbitals were divided into two sets based on their localization characteristics on either the donor or acceptor groups. We define $\boldsymbol{L_i}$ in eq. 3 as the sum of the squared coefficients ($C_{i\mu}$) of atomic orbitals χ_μ^{AO} for molecular orbital $i(\psi_i^{MO})$ to identify whether MO i is localized on the donor or acceptor,

$$\psi_i^{MO} = \sum_\mu C_{i\mu}\chi_\mu^{AO}, L_i^D = \sum_{\mu \in D} C_{i\mu}^2, \text{and} L_i^A = \sum_{\mu \in A} C_{i\mu}^2 \quad (3)$$

When L_i^D on the Fe porphyrin is larger than 0.3, MO i is identified as being localized on the donor. If L_i^A on ZnP$^{+\bullet}$Trp191 is larger than 0.3, MO i is localized on the acceptor. (Note that Trp191 is taken as part of the acceptor. See the detailed scheme in Figure S2.) We also examined other threshold values larger or smaller than 0.3 and found that values around 0.3 produce stable values of $\boldsymbol{\langle H_{DA}^2 \rangle}$.

For each pair of donor and acceptor molecular orbitals (e.g., $i \varepsilon D$ and $j \varepsilon A$), the two-state generalized Mulliken-Hush (GMH) $\boldsymbol{H_{ij}}$ value is computed by

$$H_{ij}=\frac{\mu_{ij}\Delta E_{ij}}{\sqrt{(\mu_i-\mu_j)^2+4\mu_{ij}^2}} \quad (4)$$

Here, $\boldsymbol{\Delta E_{ij}}$ is the energy gap between donor and acceptor MOs, μ_i and μ_j are the corresponding dipole moments, and μ_{ij} is the transition dipole moment between donor and acceptor. (Note that the molecule must be rotated along its dipole moment apply eq. 4, since the dipole is a vector.) Because the energy eigenvalues for frontier MOs of the donor/acceptor are similar, the frontier MOs localized on a porphyrin exchange rapidly with structural fluctuations along the MD trajectory (see Tables S5 and S6 for the eigenvalues of frontier MOs of selected MD snapshots). The $\boldsymbol{H_{DA}}$ value for one MD snapshot is computed by summing over all donor-acceptor MO pairs,

$$H_{DA}=\sum_{i\in D_{MO}}^{N_D}\sum_{j\in A_{MO}}^{N_A} H_{ij}. \quad (5)$$

Here, H_{ij} is the electronic coupling between one donor molecular orbital and one acceptor molecular orbital. N_D is the number of frontier molecular orbitals localized on the heme donor and N_D is the number of frontier molecular orbitals localized on the $ZnP^{+\bullet}$Trp191 acceptor. We computed $\langle \boldsymbol{H_{DA}^2} \rangle$ using the last 2,000 snapshots from the MD simulations of the five CcP:Cc complexes with eqs. 4 and 5.

D. ESP charge fitting analysis

We used the Gaussian 03 program[84] with the B3LYP/6–31G* approach[85–97] to compute the ESP charges on the ZnP including W191. Ten representative geometries of ZnP were taken from the MD simulations: five with larger $|\boldsymbol{H_{DA}}|$ values (~10^{-5} eV) and five with smaller $|\boldsymbol{H_{DA}}|$ values (~10^{-8} eV). ESP charges were fitted for the neutral singlet spin states of ZnP and also for the doublet cation radicals of ZnP. ESP charge differences between the two states are shown in Table S2. These charges were used to characterize the localization of the holes on W191.

E. Reorganization energy calculations

Reorganization energies were computed using the finite difference Poisson-Boltzmann (FDPB) method implemented in the DelPhi software package.[75,98–101] A 161×161×161 grid is sufficient to obtain converged λ values. The linearized PB equation with Debye-Hükel boundary conditions was solved to obtain $\delta\phi_i^{d*d}$ and $\delta\phi_i^{ad}$ in eq. 6. The convergence criterion is $\mathbf{1 \times 10^{-4}}$ kT/e total residual error in the potential. Here, $\delta\phi_i^{d*d}$ is the accompanying change in the potential due to re-equilibration of the electronic polarization, and $\delta\phi_i^{ad}$ is the change in the potential upon electron transfer.

The ESP charges (i.e., q_i^{ad} in eq. 6) on the donor and acceptor were calculated separately using Gaussian 09[102] at the Hartree-Fock level with a 6–31+G(d) basis set using crystal structures of the five protein-protein complexes. A dielectric constant of 2 (representing electronic polarizability) was assigned to the protein and solvent, and an ionic strength was set to zero to obtain $\delta\phi_i^{d*d}$. Static dielectric constants of 4 and 80 were then assigned to the protein and solvent, respectively, and the experimental ionic strength of 6 mM[18] was used to

compute $\delta\phi_i^{ad}$.[75] λ was calculated using eq. 6 by summing over the product of the charge and the potentials on the donor and acceptor group atoms,

$$\lambda = \frac{1}{2}\sum_i \left(\delta\phi_i^{d*d} - \delta\phi_i^{ad}\right) dq_i^{ad} \quad (6)$$

Results and Discussion

Changes in the Heme-ZnP $\langle H_{DA}^2 \rangle$ values with protein-protein interface structures do not explain the nearly equal observed back ET rate constants for the F82Y(I) mutants compared to the WT CcP:Cc and the F82S(W) mutants

As shown in Figure S1, the protein-protein complex geometries of F82Y and F82I Cc mutants are very different from those of the WT CcP:Cc complex,[9] with strikingly different D-A distances (see Table 1 and Figure 3). The ET distances (Fe-ZnP edge) are 22.4 Å for WT, 22.5 Å for F82W, 22.6 Å for F82S, 27.9 Å for F82Y, and 27.8 Å for F82I. Despite the fact that the two sets of DA distances differ by ~5 Å, the experimental back ET rate constants in F82Y(I) are not significantly different compared to the WT CcP:Cc complex and to the F82S(W) mutants. To explore this surprising insensitivity to complex geometry and ET distance, we computed the average donor-acceptor electronic couplings using the PATHWAY and INDO-GMH methods to determine whether specifics of the protein fold might cause rate differences not anticipated by distance analysis alone.

The relative mean-squared donor-acceptor electronic couplings from the Cc heme to the CcP ZnP computed with the PATHWAY method are given in Table 1. The logarithm of the pathway coupling strengths for WT CcP:Cc snapshots are shown in Figure 5 and the quantum chemically computed log|$\boldsymbol{H_{DA}}$| values are shown in Figure 6 (see Figure S3 for the logarithm of |$\boldsymbol{H_{DA}}$| values of the four CcP:Cc mutants). For each protein complex, the |$\boldsymbol{H_{DA}}$| values fluctuate one order of magnitude among 2,000 MD snapshots. The computed couplings for the WT CcP:Cc complex and for the F82S(W) mutants reflect the fact that WT and F82S(W) protein complexes have similar protein-protein docking geometries and ET coupling pathways. Indeed, the measured back ET rate constants are similar.[9] In contrast, F82I and F82Y (with significantly different docking conformations compared to the WT CcP:Cc complex and F82S(W) mutants) have PATHWAY computed mean-squared heme-ZnP couplings that are two orders of magnitude smaller. Such $\langle \boldsymbol{H}_{DA}^{\boldsymbol{2}} \rangle$ differences are consistent with the simple D-A distance differences among the crystal structures.

The metal-to-metal (Fe-Zn) distances for the WT CcP:Cc complex and F82S(W) based on their crystal structure are 26.5 Å, 26.4 Å and 26.3 Å, respectively; the Fe atom to ZnP edge minimum distances are 22.4 Å, 22.5 Å and 22.1 Å, respectively (See Table 1 and Figure 3). The similar distances are indeed consistent with comparable ET PATHWAY couplings for WT CcP:Cc and F82S(W). However, for the F82Y(I) mutants, the metal-to-metal distances are 29.8 Å and 29.4 Å, while the Fe-ZnP edge minimum distances are 27.9 Å and 27.8 Å, respectively (see Table 1 and Figure 3). Both the metal-to-metal and the metal-to-edge distances are about 3–5 Å larger in F82Y(I) than in the WT CcP:Cc and the F82S(W) mutants, which is expected to decrease the coupling by one to two orders of magnitude, based on square barrier estimates, and is consistent with the relative mean-squared PATHWAY couplings. Similar conclusions are obtained if we consider the heme-to-Trp $\langle \boldsymbol{H}_{DA}^{\boldsymbol{2}} \rangle$ values (see Table S3 for distance analyses of Fe-ZnP and Fe-Trp): computed mean-squared electronic couplings are very different for the two sets of proteins.

To further analyze the protein-mediated tunneling, the INDO-GMH scheme was used to compute the electronic couplings, shown in Table 2, for the back ET (Fe(II)Cc → Zn(II)CcP$^{\bullet+}$). This method could capture tunneling pathway interference effects that are included at best in an average sense within the tunneling pathway framework. Couplings obtained from INDO-GMH also decay rapidly with D-A distance, as in the PATHWAY analysis. Thus, it is puzzling why all five the protein complexes, with different D-A distances, have similar observed back ET rate constants. Next, we examine whether additional factors, such as variations in the reorganization energies, may influence the relative rates because large conformational changes occur in the protein-protein interface (*vide infra*).

In summary, the above PATHWAY analysis considered the Fe-to-ZnP back ET, while the INDO-GMH analysis includes both Fe-to-ZnP and Fe-to-Trp191 back ET mechanisms. Both the (ensemble-averaged) PATHWAY and INDO-GMH coupling analyses of the WT CcP:Cc complex and of the four mutants indicate that ET couplings decay approximately exponentially with the D-A distance. Thus, the similar back ET rates among the five protein complexes are *not* explained by coupling pathway effects between heme and ZnP(Trp191). Next, we will examine the competing single step (Fe-to-ZnP) and hopping (Fe-to-Trp191) recombination mechanisms in greater detail.

Hopping recombination via Trp191 is supported for back ET in all systems

The computed heme-to-ZnP electronic coupling trends do not explain the measured back ET rates. However, we found that MOs localized on Trp191 computed by INDO make large contributions to $\langle \boldsymbol{H}_{DA}^{2} \rangle^{1/2}$ for all five proteins. Individual MD snapshots with large deviations of $|\boldsymbol{H}_{DA}|$ from $\langle \boldsymbol{H}_{DA}^{2} \rangle^{1/2}$ in the INDO-GMH calculations indeed have several Trp191 localized frontier orbitals that contribute to $\langle \boldsymbol{H}_{DA}^{2} \rangle$. As such, eq. 5 can be divided into two parts, since the hole is spread over both ZnP and Trp191:

$$H_{DA} = H_{heme-ZnP} + H_{heme-Trp191} \quad (7)$$

In addition to direct heme-ZnP tunneling, recombination ET may also occur by incoherent sequential electron transfer via Trp191 (i.e., Fe^{II}Cc→Trp191→ ZnP$^{+\bullet}$). That is, even low populations of Trp intermediate states may have a large effect on the observed rate. Since Trp191 in CcP is ~3.6 Å (edge-to-edge) away from ZnP, the rate of Trp191 oxidation by ZnP$^{+\bullet}$ may be fast on the time-scale of ET recombination because of proximity to ZnP. Hence, back ET via incoherent Trp hopping may accelerate charge recombination[9] (see Figure 2 for the detailed kinetic scheme).

To explore in greater detail whether a hole can be localized on Trp191, if only transiently, ESP charge analysis based on density functional theory was performed. We computed ESP charge differences between the neutral and radical cation states of ZnP and Trp191. Despite the reduction in the pK_a of Trp upon oxidation, it is well established that the Trp191 radical remains protonated in the long-lived Cpd I state of CcP, and thus it should also remain so on the much shorter time-scales of the ET processes investigated here.[103] For ZnP and Trp191, the sum of the ESP charge differences between the neutral and radical cation states is shown in Table S2 for five MD snapshots with large $|\boldsymbol{H}_{DA}|$ values and for five MD snapshots with small computed $|\boldsymbol{H}_{DA}|$ values. The charge values in Table S2 for ZnP or Trp191 represent the percentage of the hole that is localized on ZnP or Trp191. For the five MD snapshots with large $|H_{DA}|$values, we find that 12% of the hole is localized on Trp191. In contrast, only 2% of the hole is localized on Trp191 for the five MD snapshots with small $|\boldsymbol{H}_{DA}|$

values. This analysis of hole localization supports the viability of a hopping mechanism via Trp191 for all of the Cc/CcP species.

To examine whether or not hopping via Trp191 is essential in determining $\langle H_{DA}^2 \rangle$ for recombination ET, we removed all of the MOs localized on Trp191 from the INDO-GMH calculations of $\langle H_{DA}^2 \rangle$ (i.e., we set $H_{heme\text{-}Trp191} = 0$ in eq. 7). As shown in Table 2, the resulting $\langle H_{DA}^2 \rangle$ values for WT CcP:Cc and for the F82S(W) mutants decreased by about three orders of magnitude compared to the values calculated with Trp191 present. The decrease in the ET rate upon removing the Trp191 in our calculations supports a hopping mechanism through Trp191 for WT CcP:Cc and F82S(W) dominating the back ET reaction. In contrast, for the F82Y(I) mutants, the $\langle H_{DA}^2 \rangle$ values are decreased around one order of magnitude by removing the Trp191.

Hoffman and coworkers showed that the W191F CcP single mutant has a much slower back ET rate ($k_{eb} = 74 s^{-1}$)[40] than WT CcP:Cc ($k_{eb} \approx 6{,}000 s^{-1}$) in solution. To further explore the role of Trp191 in the coupling and back ET, we modeled the system studied by Hoffman and coworkers[40] by building the W191F mutant based on the WT crystal structure of CcP:Cc. We mutated Trp191 of CcP to Phe191 using the VMD program.[76] Phe cannot be oxidized by $ZnP^{+\bullet}$.[9,14,40] The QM region for the INDO analysis in this mutant was based on PATHWAY screening (shown in Table S1). No orbitals among the ten highest occupied molecular orbitals were found to be localized on Phe191 in the INDO analysis. Back ET for W191F is likely to occur in one-step:

$$ZnP^{+}CcP{:}Fe^{2+}Cc \xrightarrow{k_b} ZnPCcP{:}Fe^{3+}Cc \quad (8)$$

The INDO-GMH analysis shows that the mean-squared coupling of the WT CcP:Cc complex is about 500 times larger than that of the W191F mutant, in agreement with the experimental observation that the measured back ET rate of W191F drops 200-fold compared to the WT CcP:Cc complex.[40] This further supports a hopping pathway through Trp191 in the WT CcP:Cc and F82S(W) complexes, determining the back ET mechanism and rate.

In summary, INDO-GMH and ESP charge analyses of the five protein complexes and of the mutant (W191F) indicate a crucial role for Trp191 in back ET. A multi-step hopping mechanism via Trp191 is likely to be present in all five CcP:Cc complexes, but the propensity for hole delocalization onto Trp191 does not explain the independence of the recombination rates on distance. In fact, hopping recombination would seem to enhance the rates in the shorter distance systems compared to the longer distance systems, further widening the expected gap between recombination ET rates.

Trp191 plays a larger role in the WT complex and F82S(W) mutants than in F82Y(I) based on INDO-GMH analysis

Why does Trp191 play a less significant role in determining $\langle H_{DA}^2 \rangle$ in F82Y(I) than in the WT CcP:Cc and F82S(W), as shown in Table 2? To address this question, we chose three MD snapshots randomly with large $|H_{DA}|$ values and three MD snapshots with small $|H_{DA}|$ values for each of the five protein complexes. The frontier molecular orbitals with the largest contribution to $\langle H_{DA}^2 \rangle$ are plotted in Figure S6. Large $|H_{DA}|$ snapshots always have strong heme-Trp191 mixing (hopping recombination) while MD snapshots with small $|H_{DA}|$ values always have weaker heme-ZnP mixing (single step tunneling recombination). As shown in Figure S7 and Table S4, strong coupling between heme and Trp191 occurs in

fewer than 1% of the 2,000 snapshots for the F82Y(I) mutants. In contrast, strong coupling between heme and Trp191 occurs for more than 10% of 2,000 snapshots in the WT CcP:Cc and F82S(W) complexes and makes significant contributions to the total $\langle \boldsymbol{H}^{\boldsymbol{2}}_{\boldsymbol{DA}} \rangle$ values. Note that since the heme-Trp191 distances in the five protein complexes are about 7 Å shorter than the heme-to-ZnP distances (Figure 3), the heme-to-Trp191 coupling is always about three orders of magnitude larger than the heme-to-ZnP coupling, based on an average exponential distance decay model. Nevertheless, taking F82Y as an example, only 0.7% of the snapshots (i.e., N_{Trp}/N_{tot}, N_{Trp} is the number of snapshots in which the frontier molecular orbital were localized on Trp191 and N_{tot} is the total number of snapshots, Table S4) have Trp191 localized (acceptor) frontier orbitals, and the heme-to-Trp191 coupling accounts for about 87.5% of the total coupling (i.e., $\langle H^2_{Fe-Trp} \rangle / \langle H^2_{D-A} \rangle$, where $\langle H^2_{Fe-Trp} \rangle$ is the mean-squared ET coupling of Fe-Trp191 and $\langle H^2_{D-A} \rangle$ is the total mean-squared ET coupling). However, for F82W, 11.6% (N_{Trp}/N_{tot}, Table S4) of the snapshots have strong heme-to-Trp 191 coupling that accounts for about 99.9% ($\langle H^2_{Fe-Trp} \rangle / \langle H^2_{D-A} \rangle$) of the total coupling. Therefore, eliminating Trp191 in F82Y(I) would result in an averaged squared ET coupling becoming about one order of magnitude smaller; eliminating Trp191 in F82S(W) would cause a two order of magnitude decrease in a mean-squared ET coupling.

Why are the percentages of snapshots with the Trp191 localized frontier orbitals so different for the WT and F82S(W) mutants compared to the F82Y(I) mutants? Mutations at the protein-protein interface cause large conformational changes in F82Y(I), orienting the positively charged Lys 77 and Lys 84 residues of Cc at the interface to enter the ET coupling pathways (this does not occur in the WT and F82S(W) species). The electrostatic interactions of the two Lys residues in the ET pathway of the F82Y(I) mutants perturb the energy ordering of the frontier molecular orbitals. Indeed, we analyzed the energy eigenvalues of the ten frontier orbitals of the F82Y and WT complexes (frame 142 in F82Y and frame 730 in WT as two examples). As shown in Table S5, frame 142 in F82Y (Lys positively charged) has much lower energy eigenvalues of frontier orbitals compared with frame 730 in WT. In particular, several orbitals localized on ZnP are shifted into the set of the ten highest energy occupied orbitals. To test our hypothesis that the positively charged Lys residues can influence the energy ordering of the frontier orbitals, we neutralized the two Lys residues in Cc and analyzed these model systems using INDO. We found that the frontier orbitals in F82Y(I) with neutralized Lys 77 and Lys 84 are very similar to those in the WT complex, as shown in Tables S5 and S6. This indicates that the charges of residues on or near the tunneling pathways strongly influence the coupling strengths. Neutralizing the two positively charged Lys residues in F82Y shifts the energies of some of the molecular orbitals localized on the heme up into the set of the frontier orbitals. Therefore, mutations at the protein-protein interface change the ET coupling pathways, increase the back ET distance in F82Y(I), and weaken Trp191 hopping pathways compared to WT and F82S(W) species.

In summary, ~10% of the sampled WT and F82S(W) ensemble supports Trp-mediated ET re-combination, while only ~1% of the F82Y(I) ensemble supports Trp-mediated recombination. We predict that further mutation of Trp191 in F82Y(I) to residues such as Phe will lower the ET rates 10 fold because of the relatively low percentage of snapshots with strong heme-to-Trp191 ET pathways in F82Y(I). In contrast, we predict that back ET rates in the double mutants W191F CcP:F82S(W) Cc will be two to three orders of magnitude slower compared to the rates in the WT CcP:Cc complex. More interestingly, if Lys77 and Lys84 of Cc were mutated to neutral residues, the back ET rates of F82Y(I) would be predicted to increase about 100 fold (assuming the F82Y(I) docking motifs are conserved).

Increased reorganization energies in F82Y(I) accelerate back ET rates, despite their weaker $\langle H_{DA}^2 \rangle$ values

Above, we calculated $\langle H_{DA}^2 \rangle$ values for the F82Y(I) mutants to be two to three orders of magnitude smaller than $\langle H_{DA}^2 \rangle$ values for the WT CcP:Cc complex and for the F82S(W) mutants. This is explained by the longer D-A distance in the F82Y(I) mutants, as is the case as well for hopping pathways through Trp191. The computed $\langle H_{DA}^2 \rangle$ trends therefore do not explain the experimental observation that the rates in the F82Y(I) mutants are unchanged as the D-A distance increases by ~6 Å (edge-to-edge). Since the F82Y(I) mutants have large conformational changes in the protein-protein interface (compared to the WT CcP:Cc complex and F82S(W)), we suggest that the (distance-dependent) reorganization energies for these two mutants account for the ET rate similarity among the five protein complexes. Indeed, similar distance dependent λ effects have been found in other chemical systems.[104]

The Marcus two-sphere continuum model predicts:[71]

$$\lambda = (\Delta e)^2 \left[\frac{1}{\varepsilon_{op}} - \frac{1}{\varepsilon_s}\right]\left[\frac{1}{2a_1} + \frac{1}{2a_2} - \frac{1}{r}\right] \quad (9)$$

where Δe is the charge transferred from the donor to the acceptor, a_1 and a_2 are the radii of the donor and acceptor, r and is the donor-acceptor distance. ε_{op} and ε_s are the optical and static dielectric constants of the medium, respectively. Here, $\Delta e = 1$, $a_1 = 2.75$ Å and $a_2 = 6.75$ Å, which are the typical D and A radii (since we chose Fe as the donor and ZnP as the acceptor). We use $\varepsilon_{op} = 2$ and $\varepsilon_s = 4$. The Marcus model and edge-edge distances in Table 1 give the computed λ values for the five proteins shown in Table 3. Since the edge-edge distance for F82Y(I) increases by about 6 Å compared to the other three derivatives, λ increases by about 0.1 eV compared to WT CcP:Cc. (Note that the reorganization energy trends for all five proteins are not changed by the values of a_1 and a_2.) A clear limitation of the Marcus two-sphere model applied to proteins is its assumption of "spherical" donors and acceptors and its use of a single dielectric constant to describe the medium (not distinguishing between protein and solvent).

Finite difference Poisson-Boltzmann (FDPB) analysis offers some advantage over the Marcus two-sphere model (nonspherical redox species and two or more dielectric constants), although it is challenging to unambiguously assign the dielectric constants. Quantum corrections to eq. 1 cause further complications in predicting how changes in λ influence the ET rate. With these complexities in mind, we have chosen the FDPB approach as a compromise strategy (*vide infra*), given the qualitative aims of our analysis, and we use this approach to calculate the ET reorganization energies (see Table 3). Indeed, the FDPB model calculations give the same general trends in λ as does the Marcus two-sphere model. The FDPB model includes two dielectric constants, one characteristic of protein (ε=4) and one of water (ε=80). Since only one dielectric constant appears in the two-sphere Marcus model, and we have set ε=4, we believe that this implementation of the two-sphere model likely underestimates λ, and we favor the FDPB approach which accommodates two dielectric constants. Indeed, the FDPB method has seen success in estimating reorganization energies,[75] although there is uncertainty associated with the choice of these continuum dielectric constants and the geometry of the dielectric boundaries. Our main interest is in the distance scaling of λ, so we adopt the simple FDPB approach here. Other strategies to obtain more reliable estimates of λ are based on linear response theory and MD or QM/MM simulations. See, for example, studies from the groups of Warshel,[105–109] Blumberger and Klein,[42,110,111] Yang,[112] and Elstner[113] for detailed descriptions of these methods. The atomistic simulations promise enhanced reliability derived from fewer empirical parameters,

but the methods also carry a larger computational cost and may have limitations when implemented with force fields that are not polarizable. A more general discussion is beyond the general scope of the present study.

The two different reorganization energy computational protocols have very different consequences. The two-sphere computed λ values differ little (~0.1eV) across the entire suite of variants. In contrast, in the FDBP approach, as the metal-to-metal distance increases by 3 Å and the Fe-ZnP edge distance increases by about 6 Å, the computed reorganization energy increases by about 0.4 eV in the F82Y(I) mutants compared to the WT CcP:Cc complex because of the influence of the high dielectric region being included. Thus, the WT, F82W, and F82S variants have a roughly common value of λ that is 0.4 V larger – nearly double the values - than λ for the F82Y and W191F variants. This major difference in the exponential of the FC factors for the two subgroups of proteins has a dramatic impact on the computed values of the rate constants and brings the experiment and theory into qualitative alignment. Hence we discuss below only the results for the FDBP approach to computing the reorganization energy.

In the analysis of cytochrome *c*:cytochrome *c* peroxidase charge recombination discussed above, the conformational sampling is carried out on the ns timescale. Since this time scale is several orders of magnitude shorter than the time scale of the fastest charge recombination kinetics, we assumed that an ensemble-averaged recombination rate would be proportional to $\langle H_{DA}^2 \rangle$. Indeed, on the ns time scale, we observe protein snapshots with hole localization on ZnP and on Trp191 for different structural snapshots. If the experimental charge recombination kinetics contained only a single phase, we would end our analysis here. However, the observed charge re-combination kinetics is multi-phasic.[9,15,40]

Ideally, we would sample protein conformational fluctuations on the full experimental time scale, extending to hundreds of ms. However, in the absence of this capability, we construct a simple hypothesis to link the two qualitatively different hole localizing poses seen in MD to the non-exponential kinetics. That is, we will assume that the protein-protein complex is able to “lock in” hole localizing states of ZnP and of Trp191 that then undergo slow conformational exchange, thus giving rise to multi-exponential kinetics. This kind of relaxation could, for example, involve protein polarization around the hole species. Note that the MD simulations are based upon neutral ZnP/Trp191 units, and thus preclude such hole localization and trapping. As such, we estimate the time scales of the two recombination components by binning our inter-protein H_{DA} values into classes that involve heme-Trp191 tunneling (corresponding to the fast kinetic phase) and those that involve heme-ZnP tunneling (corresponding to the slow kinetic phase). To obtain the rate constant for the slow recombination phase, we used the reorganization energy of the W191F mutant and $\langle \boldsymbol{H_{DA}^2} \rangle_{\boldsymbol{heme-ZnP}}$ as the mean-squared coupling. The coupling for the fast phase is taken as $\langle \boldsymbol{H_{DA}^2} \rangle_{\boldsymbol{heme-Trp191}}$ (Table 3). The averaging is over those members of the two ensembles with stronger (heme-Trp191) and weaker (heme-ZnP) tunneling recombination. The computed back ET rates for slow- and fast-phase kinetics appear in Table 4.

For the complexes with F82Y(I), we found that the ET rate constants for both kinetic phases agree well with the observed values. Furthermore, although the electronic couplings in F82Y(I) are three orders of magnitude smaller than in the WT complex, the rate constants for the dominant fast-phase ET process are computed to be only 10 times smaller than for the WT CcP:Cc complex because the reorganization energy changes in the F82Y(I) mutants largely compensate for the weaker electronic couplings. These complexes are in the ‘inverted regime’, where the two-fold larger value of λ as calculated by the FDPB protocol

for F82Y(I) (Table 3) accelerates ET.[114] Meanwhile, the fast-phase ET in W191F disappeared in our calculations (last row of Table 4), as is also observed in the experiments.[40]

For the WT and F82S(W) complexes, the predicted ET rate constants for the slow kinetic phase are likewise in good agreement with the experimental values, Table 3. However, the predicted rate constants for the fast kinetic phase are 15–50 fold larger than the larger experimental ET rate constants. It may well be that the calculated process is not observed experimentally, and that the experiment and computation thus are disjoint. For an ET cycle with a back ET rate constant of $k_b \sim 10^5\ s^{-1}$, but a forward rate orders of magnitude slower, the accumulation of the ET intermediate would be too low to be detectable. This is indeed the case for the Cc:CcP complex in single crystals.[9] Furthermore, the contributions of Cc Lys77 and Lys84 to the calculated F82Y(I) back rates underscores the susceptibility of interprotein ET to the states of specific side chains at the interface. It is possible that similar changes in charge or conformation of the long ionizable residues in the WT interface (e.g., Cc Lys11, Cc Arg13, CcP Glu201) that are not captured by MD decrease the back rates. It is worth noting that the crystal structures of the F82S(W) variants display greater variability in Cc positioning than the WT structure.[9]

Alternatively, the difference between the predicted and experimental values of k_{b1} could indicate that even the FDPB method for computing reorganization energies is not yet sufficiently accurate and/or that the contribution of W191 to the coupling is overestimated. As the computed values of λ put the complexes with F82S(W) further from the maximum value in the Marcus model, (Table 3, using estimated redox potentials as noted[115,116]) the predicted rate constants for these mutants are more strongly dependent on λ and ΔG than the F82Y(I) mutants and are thus more sensitive to model-dependent uncertainties associated with the FDPB approach for computing λ.

Conclusions

We have used electronic coupling and reorganization energy analysis to explore the mechanisms of charge recombination in WT and mutant CcP:Cc protein complexes. Our analysis suggests that the charge recombination involves a mixed tunneling-hopping mechanism in all five protein complexes, consistent with earlier suggestions and multiphasic back ET observations.[9,39] Interestingly, electrostatic interactions of the Trp cation radical with nearby Lys diminish the contributions of hole hopping in F82Y(I) mutants by 10 fold compared to the WT and F82S(W) mutants. Hole hopping via Trp191 accelerates the recombination kinetics by shortening the tunneling distance. It is particularly intriguing that the Trp 191 establishes “flickering” resonances as the protein undergoes conformational changes, a dynamical control of electronic structure that we have also noted for hole transport in nucleic acids.[7,117]

Similar recombination rate constants are found for all five protein complexes, despite the very large distance and conformational differences in the F82Y(I) species compared to the WT and F82S(W) mutants. Our computations suggest that increasing the reorganization energy in the F82Y(I) mutants accelerates recombination ET, because this reaction is in the inverted region, changes in λ compensate the lower population of hopping pathways and the longer D-A distance in the F82Y(I) mutants. The similarity of rate constants observed for all five protein-protein complexes is attributed to this balance of λ, distance, and hopping pathway population effects.

Based on the hopping mechanism via Trp191 proposed in all five species, the hopping poses in WT and F82S(W) are more highly populated than in F82Y(I) (10% vs 1%). The squared

electronic couplings from the Cc heme to the CcP Trp191 are thus expected to be as much three orders of magnitude larger than from heme to ZnP (based on an exponential distance decay model, Figure 3). As such, we predict that the double mutant W191F CcP:F82Y(I) Cc complex would have an ET rate one order of magnitude smaller than that found in the F82Y(I) single mutants because only about 1% of the snapshots have frontier orbitals localized on Trp191 (Table S4).

Our calculations of electronic couplings predict that the double mutant W191F CcP:F82S(W) Cc complexes are expected to have rates slower by two orders of magnitude compared with rates of the F82S(W) mutants because about 10% of the snapshots have frontier orbital localized on Trp191 (Table S4). Because of the structural similarity between Phe and Tyr, the W191Y mutant would have very similar back ET rates compared to the W191F mutant.[39] Since Lys77 and Lys84 of Cc in F82Y(I) influence the weighting of Trp191 hopping pathway, the back ET rates are predicted to increase about 100 fold if both Lys residues are mutated to neutral residues. These proposed mutations studies offer an opportunity to explore the contribution of hole hopping to the inter-protein charge recombination mechanism in CcP:Cc complexes.

Supplementary Material

Refer to Web version on PubMed Central for supplementary material.

Acknowledgments

Support from the National Institutes of Health (GM-048043 to DNB; HL063203 to BMH) and the National Science Foundation (CHE-0749997 to BRC) is greatly appreciated.

Funding Sources

National Institutes of Health (NIH GM-048043); National Science Foundation (CHE-0749997).

References

1. Bendall, DS. Protein Electron Transfer. Oxford: Bios Scientific Publishers; 1996.
2. Lippard, SJ.; Berg, JM. Principles of Bioinorganic Chemistry. Mill Valley, Calif.: University Science Books; 1994.
3. Bertini, I.; Gray, HB.; Stiefel, E.; Valentine, JS. Biological Inorganic Chemistry. Mill Valley, CA: University Science Books; 2007.
4. Balzani, V., editor. Electron Transfer in Chemistry. New York: Wiley-VCH: Weinheim; 2001.
5. Gray HB, Winkler JR. Electron Tunneling through Proteins. Q. Rev. Biophys. 2003; 36:341–372. [PubMed: 15029828]
6. Beratan DN, Skourtis SS. Electron Transfer Mechanisms. Curr. Opin. Chem. Biol. 1998; 2:235–243. [PubMed: 9667934]
7. Beratan DN, Skourtis SS, Balabin IA, Balaeff A, Keinan S, Venkatramani R, Xiao DQ. Steering Electrons on Moving Pathways. Acc. Chem. Res. 2009; 42:1669–1678. [PubMed: 19645446]
8. Skourtis SS, Waldeck DH, Beratan DN. Fluctuations in Biological and Bioinspired Electron-Transfer Reactions. Annu. Rev. Phys. Chem. 2010; 61:461–485. [PubMed: 20192814]
9. Kang SA, Crane BR. Effects of Interface Mutations on Association Modes and Electron-Transfer Rates between Proteins. Proc. Natl. Acad. Sci. U.S.A. 2005; 102:15465–15470. [PubMed: 16227441]
10. Pletneva EV, Fulton DB, Kohzuma T, Kostic NM. Protein Docking and Gated Electron-Transfer Reactions between Zinc Cytochrome *c* and the New Plastocyanin from the Fern *Dryopteris Crassirhizoma*. Direct Kinetic Evidence for Multiple Binary Complexes. J. Am. Chem. Soc. 2000; 122:1034–1046.

11. Nocek JM, Zhou JS, DeForest S, Priyadarshy S, Beratan DN, Onuchic JN, Hoffman BM. Theory and Practice of Electron Transfer within Protein-Protein Complexes: Application to the Multidomain Binding of Cytochrome *c* by Cytochrome *c* Peroxidase. Chem. Rev. 1996; 96:2459–2489. [PubMed: 11848833]
12. Mei HK, Wang KF, Peffer N, Weatherly G, Cohen DS, Miller M, Pielak G, Durham B, Millett F. Role of Configurational Gating in Intracomplex Electron Transfer from Cytochrome *c* to the Radical Cation in Cytochrome *c* Peroxidase. Biochemistry. 1999; 38:6846–6854. [PubMed: 10346906]
13. Liang ZX, Kurnikov IV, Nocek JM, Mauk AG, Beratan DN, Hoffman BM. Dynamic Docking and Electron-Transfer between Cytochrome b(5) and a Suite of Myoglobin Surface-Charge Mutants. Introduction of a Functional-Docking Algorithm for Protein-Protein Complexes. J. Am. Chem. Soc. 2004; 126:2785–2798. [PubMed: 14995196]
14. Hoffman BM, Celis LM, Cull DA, Patel AD, Seifert JL, Wheeler KE, Wang JY, Yao J, Kurnikov IV, Nocek JM. Differential Influence of Dynamic Processes on Forward and Reverse Electron Transfer across a Protein-Protein Interface. Proc. Natl. Acad. Sci. U.S.A. 2005; 102:3564–3569. [PubMed: 15738411]
15. Xiong P, Nocek JM, Vura-Weis J, Lockard JV, Wasielewski MR, Hoffman BM. Faster Interprotein Electron Transfer in a Myoglobin, b_5 Complex with a Redesigned Interface. Science. 2010; 330:1075–1078. [PubMed: 21097931]
16. Grove TZ, Kostic NM. Metalloprotein Association, Self-Association, and Dynamics Governed by Hydrophobic Interactions: Simultaneous Occurrence of Gated and True Electron-Transfer Reactions between Cytochrome *f* and Cytochrome c_6 from Chlamydomonas Reinhardtii. J. Am. Chem. Soc. 2003; 125:10598–10607. [PubMed: 12940743]
17. Andrew SM, Thomasson KA, Northrup SH. Simulation of Electron-Transfer Self-Exchange in Cytochrome *c* and Cytochrome- b_5. J. Am. Chem. Soc. 1993; 115:5516–5521.
18. Everest AM, Wallin SA, Stemp EDA, Nocek JM, Mauk AG, Hoffman BM. Aromatic Hole Superexchange through Position-82 of Cytochrome *c* Is Not Required for Intracomplex Electron-Transfer to Zinc Cytochrome-c Peroxidase. J. Am. Chem. Soc. 1991; 113:4337–4338.
19. Niki K, Hardy WR, Hill MG, Li H, Sprinkle JR, Margoliash E, Fujita K, Tanimura R, Nakamura N, Ohno H, et al. Coupling to Lysine-13 Promotes Electron Tunneling through Carboxylate-Terminated Alkanethiol Self-Assembled Monolayers to Cytochrome c. J. Phys. Chem. B. 2003; 107:9947–9949.
20. Ren Y, Wang WH, Wang YH, Case M, Qian W, McLendon G, Huang ZX. Mapping the Electron Transfer Interface between Cytochrome b_5 and Cytochrome c. Biochemistry. 2004; 43:3527–3536. [PubMed: 15035623]
21. Zhou JS, Tran ST, McLendon G, Hoffman BM. Photoinduced Electron Transfer between Cytochrome *c* Peroxidase (D37K) and Zn-Substituted Cytochrome c: Probing the Two-Domain Binding and Reactivity of the Peroxidase. J. Am. Chem. Soc. 1997; 119:269–277.
22. Davidson VL. What Controls the Rates of Interprotein Electron-Transfer Reactions. Acc. Chem. Res. 2000; 33:87–93. [PubMed: 10673316]
23. Davidson VL. Protein Control of True, Gated, and Coupled Electron Transfer Reactions. Acc. Chem. Res. 2008; 41:730–738. [PubMed: 18442271]
24. Pelletier H, Kraut J. Crystal-Structure of a Complex between Electron-Transfer Partners, Cytochrome *c* Peroxidase and Cytochrome c. Science. 1992; 258:1748–1755. [PubMed: 1334573]
25. Erman JE, Vitello LB. Yeast Cytochrome *c* Peroxidase: Mechanistic Studies Via Protein Engineering. BBA - Prot. Struct. M. 2002; 1597:193–220.
26. Volkov AN, Nicholls P, Worrall JAR. The Complex of Cytochrome *c* and Cytochrome *c* Peroxidase: The End of the Road? BBA - Bioenergetics. 2011; 1807:1482–1503. [PubMed: 21820401]
27. Battistuzzi G, Bellei M, Bortolotti CA, Sola M. Redox Properties of Heme Peroxidases. Arch. Biochem. Biophys. 2010; 500:21–36. [PubMed: 20211593]
28. Gray HB, Winkler JR. Long-Range Electron Transfer. Proc. Natl. Acad. Sci. U.S.A. 2005; 102:3534–3539. [PubMed: 15738403]

29. Ponce A, Gray HB, Winkler JR. Electron Tunneling through Water: Oxidative Quenching of Electronically Excited Ru(Tpy)(2)(2+) (Tpy=2,2 ': 6,2 "-Terpyridine) by Ferric Ions in Aqueous Glasses at 77 K. J. Am. Chem. Soc. 2000; 122:8187–8191.
30. Hopfield JJ. Electron-Transfer between Biological Molecules by Thermally Activated Tunneling. Proc. Natl. Acad. Sci. U.S.A. 1974; 71:3640–3644. [PubMed: 16592178]
31. Kang SA, Marjavaara PJ, Crane BR. Electron Transfer between Cytochrome *c* and Cytochome c Peroxidase in Single Crystals. J. Am. Chem. Soc. 2004; 126:10836–10837. [PubMed: 15339156]
32. Sancar A. Structure and Function of DNA Photolyase and Cryptochrome Blue-Light Photoreceptors. Chem. Rev. 2003; 103:2203–2237. [PubMed: 12797829]
33. Noy D, Moser CC, Dutton PL. Design and Engineering of Photosynthetic Light-Harvesting and Electron Transfer Using Length, Time, and Energy Scales. BBA - Bioenergetics. 2006; 1757:90–105. [PubMed: 16457774]
34. Wei CC, Crane BR, Stuehr DJ. Tetrahydrobiopterin Radical Enzymology. Chem. Rev. 2003; 103:2365–2383. [PubMed: 12797834]
35. Stubbe J, Nocera DG, Yee CS, Chang MCY. Radical Initiation in the Class I Ribonucleotide Reductase: Long-Range Proton-Coupled Electron Transfer? Chem. Rev. 2003; 103:2167–2201. [PubMed: 12797828]
36. Seyedsayamdost MR, Reece SY, Nocera DG, Stubbe J. Mono-, Di-, Tri-, and Tetra-Substituted Fluorotyrosines: New Probes for Enzymes That Use Tyrosyl Radicals in Catalysis. J. Am. Chem. Soc. 2006; 128:1569–1579. [PubMed: 16448128]
37. Liang N, Mauk AG, Pielak GJ, Johnson JA, Smith M, Hoffman BM. Regulation of Interprotein Electron-Transfer by Residue-82 of Yeast Cytochrome *c*. Science. 1988; 240:311–313. [PubMed: 2832950]
38. Di Bilio AJ, Crane BR, Wehbi WA, Kiser CN, Abu-Omar MM, Carlos RM, Richards JH, Winkler JR, Gray HB. Properties of Photogenerated Tryptophan and Tyrosyl Radicals in Structurally Characterized Proteins Containing Rhenium(I) Tricarbonyl Diimines. J. Am. Chem. Soc. 2001; 123:3181–3182. [PubMed: 11457048]
39. Shih C, Museth AK, Abrahamsson M, Blanco-Rodriguez AM, Di Bilio AJ, Sudhamsu J, Crane BR, Ronayne KL, Towrie M, Vlcek A, et al. Tryptophan-Accelerated Electron Flow through Proteins. Science. 2008; 320:1760–1762. [PubMed: 18583608]
40. Seifert JL, Pfister TD, Nocek JM, Lu Y, Hoffman BM. Hopping in the Electron-Transfer Photocycle of the 1: 1 Complex of Zn-Cytochrome *c* Peroxidase with Cytochrome *c*. J. Am. Chem. Soc. 2005; 127:5750–5751. [PubMed: 15839648]
41. Debler EW, Kaufmann GF, Meijler MM, Heine A, Mee JM, Pljevaljcic G, Di Bilio AJ, Schultz PG, Millar DP, Janda KD, et al. Deeply Inverted Electron-Hole Recombination in a Luminescent Antibody-Stilbene Complex. Science. 2008; 319:1232–1235. [PubMed: 18309081]
42. Blumberger J, Klein ML. Reorganization Free Energies for Long-Range Electron Transfer in a Porphyrin-Binding Four-Helix Bundle Protein. J. Am. Chem. Soc. 2006; 128:13854–13867. [PubMed: 17044714]
43. Treutlein H, Schulten K, Brunger AT, Karplus M, Deisenhofer J, Michel H. Chromophore Protein Interactions and the Function of the Photosynthetic Reaction Center - a Molecular-Dynamics Study. Proc. Natl. Acad. Sci. U.S.A. 1992; 89:75–79. [PubMed: 1729721]
44. Parson WW, Chu ZT, Warshel A. Reorganization Energy of the Initial Electron-Transfer Step in Photosynthetic Bacterial Reaction Centers. Biophys. J. 1998; 74:182–191. [PubMed: 9449321]
45. Zeng XC, Hu H, Hu XQ, Cohen AJ, Yang WT. Ab Initio Quantum Mechanical/Molecular Mechanical Simulation of Electron Transfer Process: Fractional Electron Approach. J. Chem. Phys. 2008; 128
46. Cascella M, Magistrato A, Tavernelli I, Carloni P, Rothlisberger U. Role of Protein Frame and Solvent for the Redox Properties of Azurin from *Pseudomonas Aeruginosa*. Proc. Natl. Acad. Sci. U.S.A. 2006; 103:19641–19646. [PubMed: 17179046]
47. Petruk AA, Bartesaghi S, Trujillo M, Estrin DA, Murgida D, Kalyanaraman B, Marti MA, Radi R. Molecular Basis of Intramolecular Electron Transfer in Proteins During Radical-Mediated Oxidations: Computer Simulation Studies in Model Tyrosine-Cysteine Peptides in Solution. Arch. Biochem. Biophys. 2012; 525:82–91. [PubMed: 22640642]

48. Alvarez-Paggi D, Martin DF, DeBiase PM, Hildebrandt P, Marti MA, Murgida DH. Molecular Basis of Coupled Protein and Electron Transfer Dynamics of Cytochrome *c* in Biomimetic Complexes. J. Am. Chem. Soc. 2010; 132:5769–5778. [PubMed: 20361782]
49. Kobayashi C, Baldridge K, Onuchic JN. Multiple Versus Single Pathways in Electron Transfer in Proteins: Influence of Protein Dynamics and Hydrogen Bonds. J. Chem. Phys. 2003; 119:3550–3558.
50. Kurnikov IV, Beratan DN. Ab Initio Based Effective Hamiltonians for Long-Range Electron Transfer: Hartree-Fock Analysis. J. Chem. Phys. 1996; 105:9561–9573.
51. Liang CX, Newton MD. Ab Initio Studies of Electron-Transfer - Pathway Analysis of Effective Transfer Integrals. J. Phys. Chem. 1992; 96:2855–2866.
52. Newton MD. Thermal and Optical Electron Transfer Involving Transition Metal Complexes: Insights from Theory and Computation. Coord. Chem. Rev. 2003; 238:167–185.
53. Onuchic JN, Beratan DN, Hopfield JJ. Some Aspects of Electron-Transfer Reaction Dynamics. J. Phys. Chem. 1986; 90:3707–3721.
54. Regan JJ, Dibilio AJ, Langen R, Skov LK, Winkler JR, Gray HB, Onuchic JN. Electron-Tunneling in Azurin - the Coupling across a Beta-Sheet. Chem. Biol. 1995; 2:489–496. [PubMed: 9383451]
55. Wolfgang J, Risser SM, Priyadarshy S, Beratan DN. Secondary Structure Conformations and Long Range Electronic Interactions in Oligopeptides. J. Phys. Chem. B. 1997; 101:2986–2991.
56. Jones ML, Kurnikov IV, Beratan DN. The Nature of Tunneling Pathway and Average Packing Density Models for Protein-Mediated Electron Transfer. J. Phys. Chem. A. 2002; 106:2002–2006.
57. Regan JJ, Onuchic JN. Electron-Transfer Tubes. Adv. Chem. Phys. 1999; 107:497–553.
58. Skourtis SS, Regan JJ, Onuchic JN. Electron-Transfer in Proteins - a Novel-Approach for the Description of Donor-Acceptor Coupling. J. Phys. Chem. 1994; 98:3379–3388.
59. Stuchebrukhov AA. Tunneling Currents in Long-Distance Electron Transfer Reactions. V. Effective One Electron Approximation. J. Chem. Phys. 2003; 118:7898–7906.
60. Zhang LY, Friesner RA, Murphy RB. Ab Initio Quantum Chemical Calculation of Electron Transfer Matrix Elements for Large Molecules. J. Chem. Phys. 1997; 107:450–459.
61. Zheng XH, Stuchebrukhov AA. Electron Tunneling in the His(126) Ru-Modified Azurin: Tunneling Jumps between Protein Strands Via Hydrogen Bonds. J. Phys. Chem. B. 2003; 107:9579–9584.
62. Balabin IA, Beratan DN, Skourtis SS. Persistence of Structure over Fluctuations in Biological Electron-Transfer Reactions. Phys. Rev. Lett. 2008; 101
63. Hatcher E, Balaeff A, Keinan S, Venkatramani R, Beratan DN. Pna Versus DNA: Effects of Structural Fluctuations on Electronic Structure and Hole-Transport Mechanisms. J. Am. Chem. Soc. 2008; 130:11752–11761. [PubMed: 18693722]
64. Prytkova TR, Beratan DN, Skourtis SS. Photoselected Electron Transfer Pathways in DNA Photolyase. Proc. Natl. Acad. Sci. U.S.A. 2007; 104:802–807. [PubMed: 17209014]
65. Prytkova TR, Kurnikov IV, Beratan DN. Ab Initio Based Calculations of Electron-Transfer Rates in Metalloproteins. J. Phys. Chem. B. 2005; 109:1618–1625. [PubMed: 16851133]
66. Skourtis SS, Beratan DN. Theories of Structure-Function Relationships for Bridge-Mediated Electron Transfer Reactions. Adv. Chem. Phys. 1999; 106:377–452.
67. Beratan DN, Betts JN, Onuchic JN. Protein Electron-Transfer Rates Set by the Bridging Secondary and Tertiary Structure. Science. 1991; 252:1285–1288. [PubMed: 1656523]
68. Ridley J, Zerner M. Intermediate Neglect of Differential Overlap Technique for Spectroscopy - Pyrrole and Azines. Theor. Chim. Acta. 1973; 32:111–134.
69. Cave RJ, Newton MD. Generalization of the Mulliken-Hush Treatment for the Calculation of Electron Transfer Matrix Elements. Chem. Phys. Lett. 1996; 249:15–19.
70. Cave RJ, Newton MD. Calculation of Electronic Coupling Matrix Elements for Ground and Excited State Electron Transfer Reactions: Comparison of the Generalized Mulliken-Hush and Block Diagonalization Methods. J. Chem. Phys. 1997; 106:9213–9226.
71. Marcus RA, Sutin N. Electron Transfers in Chemistry and Biology. Biochim. Biophys. Acta. 1985; 811:265–322.

72. Fox LS, Kozik M, Winkler JR, Gray HB. Gaussian Free-Energy Dependence of Electron-Transfer Rates in Iridium Complexes. Science. 1990; 247:1069–1071. [PubMed: 17800065]
73. Gunner MR, Robertson DE, Dutton PL. Kinetic-Studies on the Reaction Center Protein from Rhodopseudomonas-Sphaeroides - the Temperature and Free-Energy Dependence of Electron-Transfer between Various Quinones in the Q_a Site and the Oxidized Bacteriochlorophyll Dimer. J. Phys. Chem. 1986; 90:3783–3795.
74. Gould IR, Ege D, Moser JE, Farid S. Efficiencies of Photoinduced Electron-Transfer Reactions - Role of the Marcus Inverted Region in Return Electron-Transfer within Geminate Radical-Ion Pairs. J. Am. Chem. Soc. 1990; 112:4290–4301.
75. Sharp KA. Calculation of Electron Transfer Reorganization Energies Using the Finite Difference Poisson-Boltzmann Model. Biophys. J. 1998; 74:1241–1250. [PubMed: 9512022]
76. Humphrey W, Dalke A, Schulten K. Vmd: Visual Molecular Dynamics. J. Mol. Graph. Model. 1996; 14:33–38.
77. Phillips JC, Braun R, Wang W, Gumbart J, Tajkhorshid E, Villa E, Chipot C, Skeel RD, Kale L, Schulten K. Scalable Molecular Dynamics with Namd. J. Comput. Chem. 2005; 26:1781–1802. [PubMed: 16222654]
78. MacKerell AD, Bashford D, Bellott M, Dunbrack RL, Evanseck JD, Field MJ, Fischer S, Gao J, Guo H, Ha S, et al. All-Atom Empirical Potential for Molecular Modeling and Dynamics Studies of Proteins. J. Phys. Chem. B. 1998; 102:3586–3616.
79. Mackerell AD, Feig M, Brooks CL. Extending the Treatment of Backbone Energetics in Protein Force Fields: Limitations of Gas-Phase Quantum Mechanics in Reproducing Protein Conformational Distributions in Molecular Dynamics Simulations. J. Comput. Chem. 2004; 25:1400–1415. [PubMed: 15185334]
80. Stote RH, Karplus M. Zinc-Binding in Proteins and Solution - a Simple but Accurate Nonbonded Representation. Proteins. 1995; 23:12–31. [PubMed: 8539245]
81. Balabin IA, Hu XQ, Beratan DN. Exploring Biological Electron Transfer Pathway Dynamics with the Pathways Plugin for VMD. J. Comput. Chem. 2012; 33:906–910. [PubMed: 22298319]
82. Hoffman BM. Triplet-State Electron-Paramagnetic Resonance Studies of Zinc Porphyrins and Zinc-Substituted Hemoglobins and Myoglobins. J. Am. Chem. Soc. 1975; 97:1688–1694. [PubMed: 166113]
83. Jordan KD, Paddon-Row MN. Analysis of the Interactions Responsible for Long-Range through-Bond-Mediated Electronic Coupling between Remote Chromophores Attached to Rigid Polynorbornyl Bridges. Chem. Rev. 1992; 92:395–410.
84. Frisch MJ, Trucks GW, Schlegel HB, Scuseria GE, Robb MA, Cheeseman JR, Montgomery JA, Vreven T, Kudin KN, Burant JC, et al. Gaussian 03, Revision D.02. 2003
85. Becke AD. Density-Functional Exchange-Energy Approximation with Correct Asymptotic-Behavior. Phys. Rev. A. 1988; 38:3098–3100. [PubMed: 9900728]
86. Becke AD. Density-Functional Thermochemistry. 3. The Role of Exact Exchange. J. Chem. Phys. 1993; 98:5648–5652.
87. Binning RC, Curtiss LA. Compact Contracted Basis-Sets for 3rd-Row Atoms - Ga-Kr. J. Comput. Chem. 1990; 11:1206–1216.
88. Blaudeau JP, McGrath MP, Curtiss LA, Radom L. Extension of Gaussian-2 (G2) Theory to Molecules Containing Third-Row Atoms K and Ca. J. Chem. Phys. 1997; 107:5016–5021.
89. Ditchfield R, Hehre WJ, Pople JA. Self-Consistent Molecular-Orbital Methods .9. Extended Gaussian-Type Basis for Molecular-Orbital Studies of Organic Molecules. J. Chem. Phys. 1971; 54:724. -&.
90. Francl MM, Pietro WJ, Hehre WJ, Binkley JS, Gordon MS, Defrees DJ, Pople JA. Self-Consistent Molecular-Orbital Methods. 23. A Polarization-Type Basis Set for 2nd-Row Elements. J. Chem. Phys. 1982; 77:3654–3665.
91. Gordon MS. The Isomers of Silacyclopropane. Chem. Phys. Lett. 1980; 76:163–168.
92. Hariharan PC, Pople JA. Influence of Polarization Functions on Molecular-Orbital Hydrogenation Energies. Theor. Chim. Acta. 1973; 28:213–222.

93. Hehre WJ, Ditchfield R, Pople JA. Self-Consistent Molecular-Orbital Methods .12. Further Extensions of Gaussian-Type Basis Sets for Use in Molecular-Orbital Studies of Organic-Molecules. J. Chem. Phys. 1972; 56:2257–2261.
94. Lee CT, Yang WT, Parr RG. Development of the Colle-Salvetti Correlation-Energy Formula into a Functional of the Electron-Density. Phys. Rev. B. 1988; 37:785–789.
95. Petersson GA, Bennett A, Tensfeldt TG, Allaham MA, Shirley WA, Mantzaris J. A Complete Basis Set Model Chemistry. 1. The Total Energies of Closed-Shell Atoms and Hydrides of the 1st-Row Elements. J. Chem. Phys. 1988; 89:2193–2218.
96. Rassolov VA, Pople JA, Ratner MA, Windus TL. 6–31g* Basis Set for Atoms K through Zn. J. Chem. Phys. 1998; 109:1223–1229.
97. Rassolov VA, Ratner MA, Pople JA, Redfern PC, Curtiss LA. 6–31g*Basis Set for Third-Row Atoms. J. Comput. Chem. 2001; 22:976–984.
98. Nicholls A, Honig B. A Rapid Finite-Difference Algorithm, Utilizing Successive over-Relaxation to Solve the Poisson-Boltzmann Equation. J. Comput. Chem. 1991; 12:435–445.
99. Rocchia W, Alexov E, Honig B. Extending the Applicability of the Nonlinear Poisson-Boltzmann Equation: Multiple Dielectric Constants and Multivalent Ions. J. Phys. Chem. B. 2001; 105:6507–6514.
100. Rocchia W, Sridharan S, Nicholls A, Alexov E, Chiabrera A, Honig B. Rapid Grid-Based Construction of the Molecular Surface and the Use of Induced Surface Charge to Calculate Reaction Field Energies: Applications to the Molecular Systems and Geometric Objects. J. Comput. Chem. 2002; 23:128–137. [PubMed: 11913378]
101. Sharp KA. Electrostatic Interactions in Macromolecules. Curr. Opin. Struct. Biol. 1994; 4:234–239.
102. Frisch MJ, Trucks GW, Schlegel HB, Scuseria GE, Robb MA, Cheeseman JR, Scalmani G, Barone V, Mennucci B, Petersson GA, et al. Gaussian 09, Revision A.1. 2009
103. Huyett JE, Doan PE, Gurbiel R, Houseman ALP, Sivaraja M, Goodin DB, Hoffman BM. Compound Es of Cytochrome-c Peroxidase Contains a Trp Pi-Cation Radical -Characterization by CW and Pulsed Q-Band Endor Spectroscopy. J. Am. Chem. Soc. 1995; 117:9033–9041.
104. Kurnikov IV, Zusman LD, Kurnikova MG, Farid RS, Beratan DN. Structural Fluctuations, Spin, Reorganization Energy, and Tunneling Energy Control of Intramolecular Electron Transfer: The Surprising Case of Electron Transfer in a d^8-d^8 Bimetallic System. J. Am. Chem. Soc. 1997; 119:5690–5700.
105. Warshel A. Dynamics of Reactions in Polar-Solvents - Semi-Classical Trajectory Studies of Electron-Transfer and Proton-Transfer Reactions. J. Phys. Chem. 1982; 86:2218–2224.
106. Hwang JK, Warshel A. Microscopic Examination of Free-Energy Relationships for Electron-Transfer in Polar-Solvents. J. Am. Chem. Soc. 1987; 109:715–720.
107. Churg AK, Warshel A. Control of the Redox Potential of Cytochrome *c* and Microscopic Dielectric Effects in Proteins. Biochemistry. 1986; 25:1675–1681. [PubMed: 3011070]
108. Warshel A, Parson WW. Computer-Simulations of Electron-Transfer Reactions in Solution and in Photosynthetic Reaction Centers. Annu. Rev. Phys. Chem. 1991; 42:279–309. [PubMed: 1747189]
109. Muegge I, Qi PX, Wand AJ, Chu ZT, Warshel A. The Reorganization Energy of Cytochrome *c* Revisited. J. Phys. Chem. B. 1997; 101:825–836.
110. Blumberger J, Lamoureux G. Reorganization Free Energies and Quantum Corrections for a Model Electron Self-Exchange Reaction: Comparison of Polarizable and Non-Polarizable Solvent Models. Mol. Phys. 2008; 106:1597–1611.
111. Tipmanee V, Oberhofer H, Park M, Kim KS, Blumberger J. Prediction of Reorganization Free Energies for Biological Electron Transfer: A Comparative Study of Ru-Modified Cytochromes and a 4-Helix Bundle Protein. J. Am. Chem. Soc. 2010; 132:17032–17040. [PubMed: 21053902]
112. Zeng XC, Hu XQ, Yang WT. Fragment-Based Quantum Mechanical/Molecular Mechanical Simulations of Thermodynamic and Kinetic Process of the Ru2+–Ru3+ Self-Exchange Electron Transfer. J. Chem. Theory and Comput. 2012; 8:4960–4967. [PubMed: 23682243]

113. Heck A, Woiczikowski PB, Kubar T, Giese B, Elstner M, Steinbrecher TB. Charge Transfer in Model Peptides: Obtaining Marcus Parameters from Molecular Simulation. J. Phys. Chem. B. 2012; 116:2284–2293. [PubMed: 22260641]

114. Mines GA, Bjerrum MJ, Hill MG, Casimiro DR, Chang IJ, Winkler JR, Gray HB. Rates of Heme Oxidation and Reduction in Ru(His33)Cytochrome *c* at Very High Driving Forces. J. Am. Chem. Soc. 1996; 118:1961–1965.

115. Rafferty SP, Pearce LL, Barker PD, Guillemette JG, Kay CM, Smith M, Mauk AG. Electrochemical, Kinetic, and Circular Dichroic Consequences of Mutations at Position-82 of Yeast Iso-1-Cytochrome *c*. Biochemistry. 1990; 29:9365–9369. [PubMed: 2174257]

116. Ho PS, Sutoris C, Liang N, Margoliash E, Hoffman BM. Species Specificity of Long-Range Electron-Transfer within the Complex between Zinc-Substituted Cytochrome *c* Peroxidase and Cytochrome *c*. J. Am. Chem. Soc. 1985; 107:1070–1071.

117. Venkatramani R, Keinan S, Balaeff A, Beratan DN. Nucleic Acid Charge Transfer: Black, White and Gray. Coord. Chem. Rev. 2011; 255:635–648. [PubMed: 21528017]

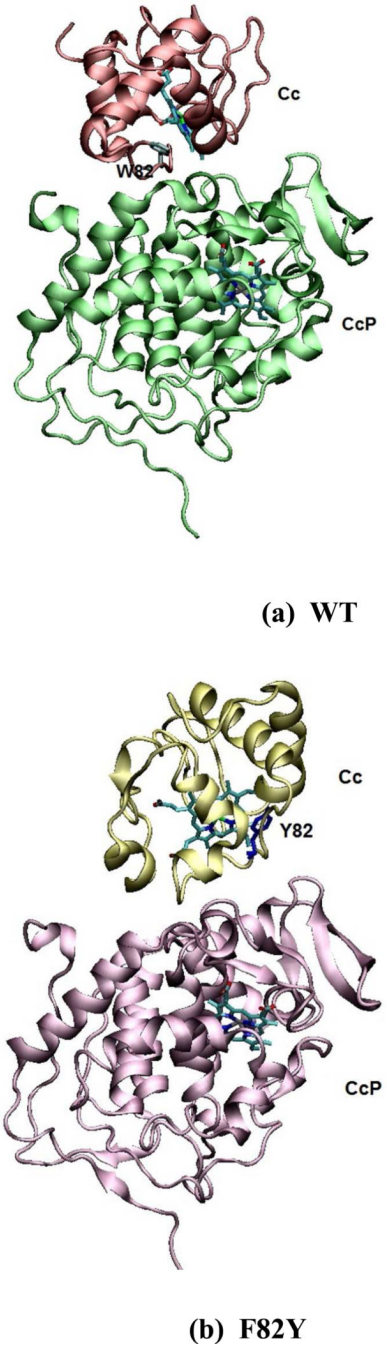

Figure 1.

Crystal structures of WT ZnCcP:Cc (PDB ID: 1U74[9]) and F82Y mutant of Cc (PDB ID: 2B12[9]). ZnP replaces the heme in CcP. Residue 82 is the mutation position in Cc. The aligned crystal structures for all five protein complexes appear in Figure S1.

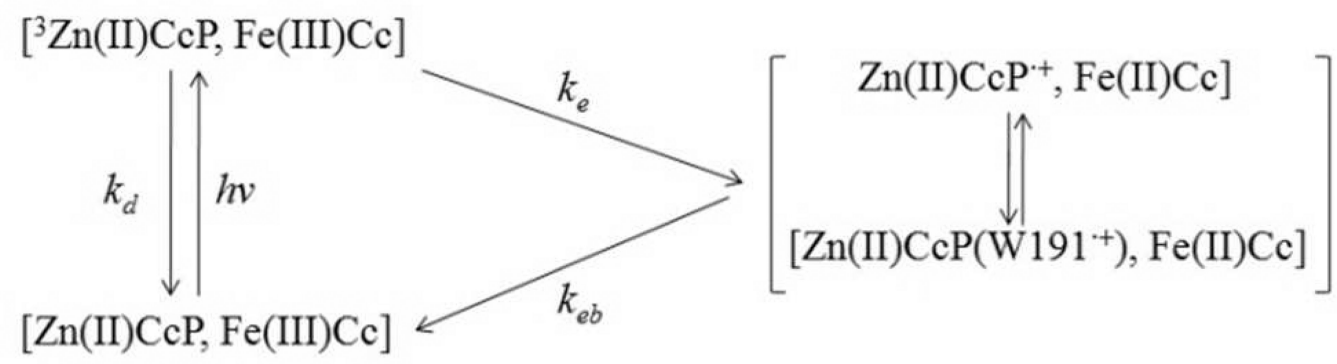

Figure 2.
The kinetic scheme for ZnCcP:Cc ET. The back ET rate constant k_{eb} studied here is insensitive to mutations that change the protein-protein interfaces and the donor-acceptor distances.

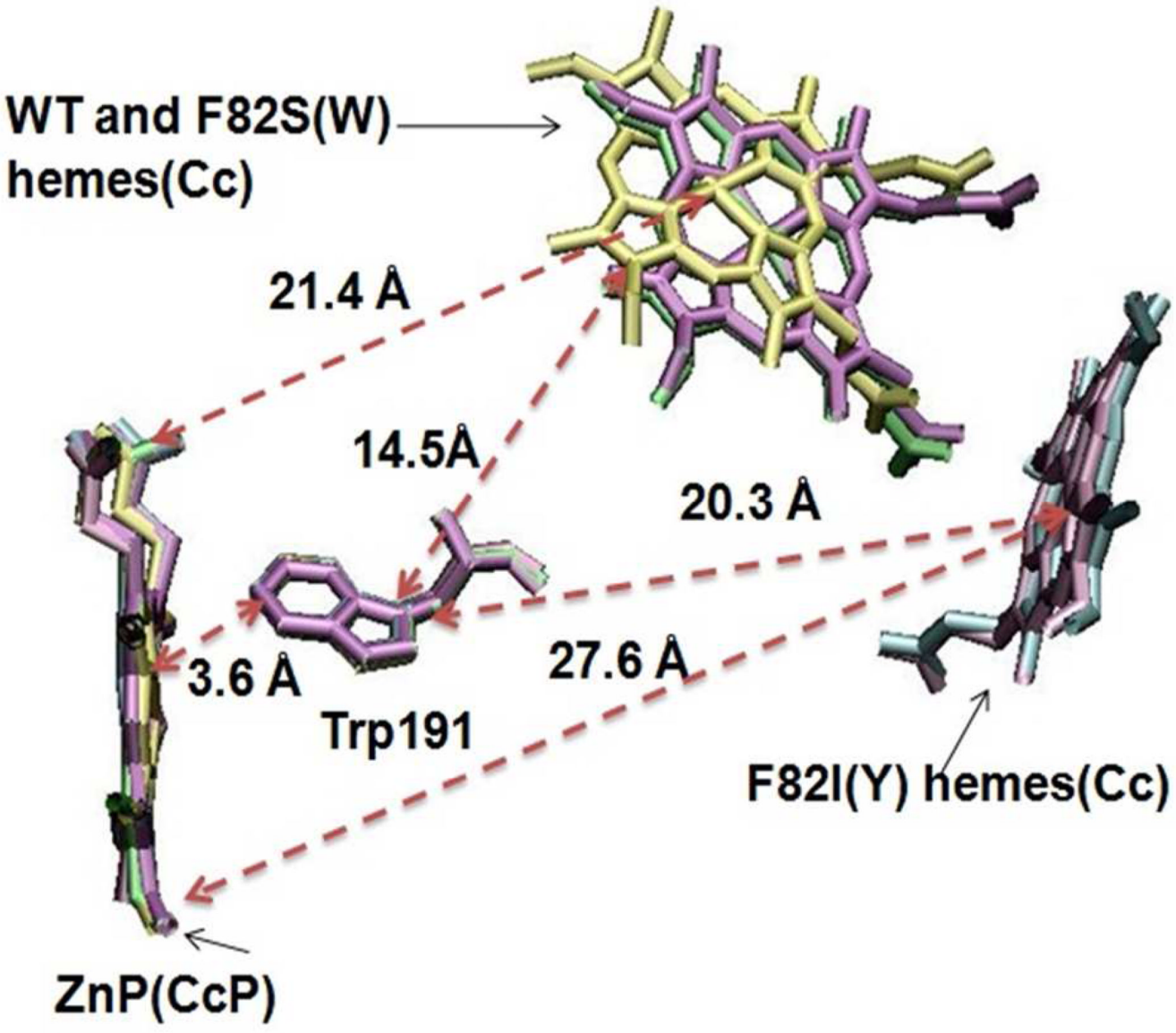

Figure 3.

The key distances in the WT CcP:Cc complex are shown in green, F82S in yellow, F82W in purple, F82Y in mauve, and F82I in cyan. The Fe-ZnP distances are 21.4 Å in WT and F82S(W) and 27.6 Å in F82Y(I). The distance of heme to Trp-191 (14.5 Å in WT and F82S(W) and 20.3 Å in F82Y(I)) is measured as the distance of Fe atom in heme to the edge of the aromatic ring in Trp191. The crystal structures are realigned on CcP using VMD[76] and only the porphyrin rings and Trp191 are shown.

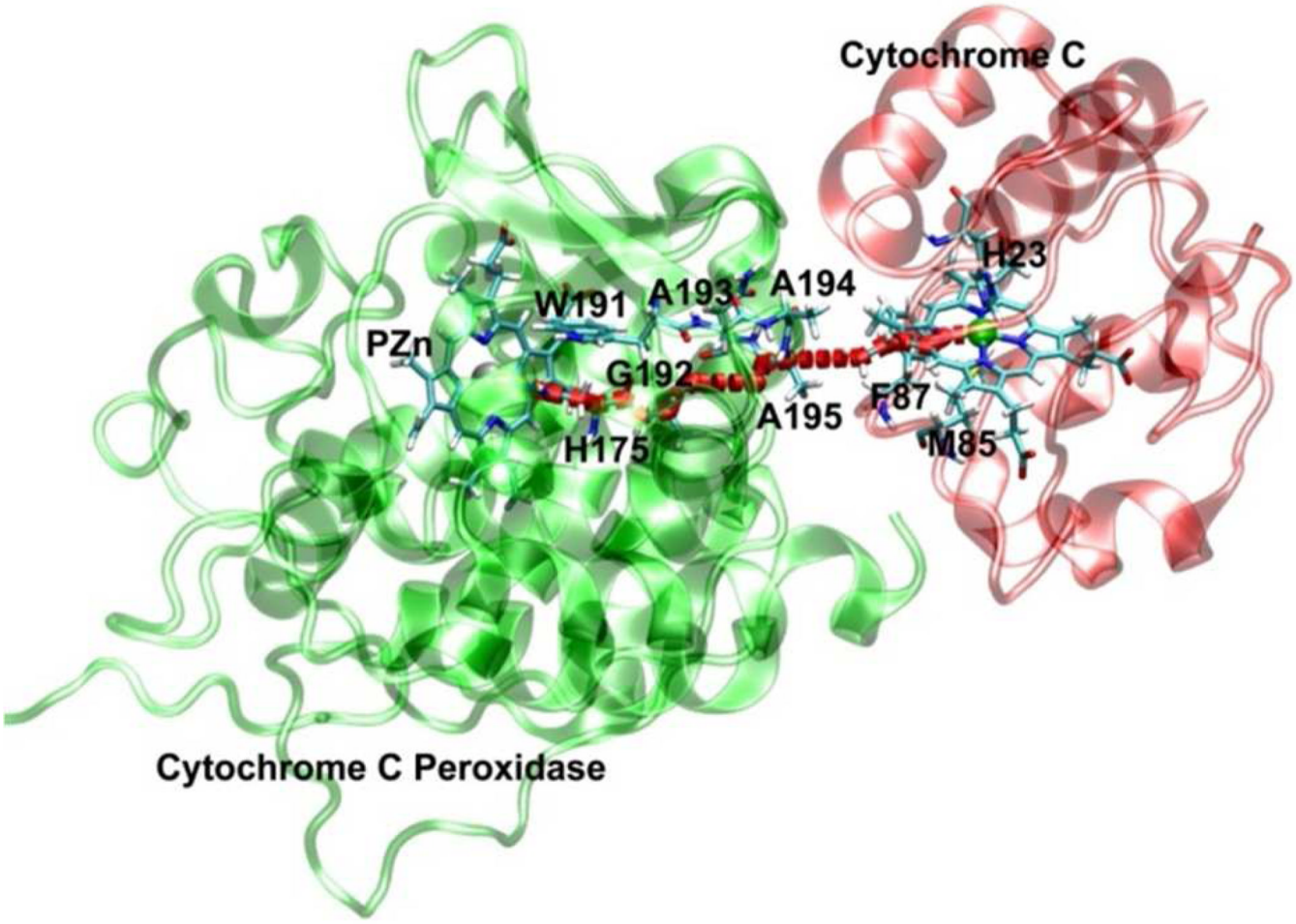

Figure 4.

Crystal structure of the WT CcP:Cc complex (PDB ID: 1U74[9]). The strongest electron-transfer pathway computed by the PATHWAY model is shown between Cc and CcP with the red dotted line. All of the labeled residues are included in the INDO calculations for the WT CcP:Cc.

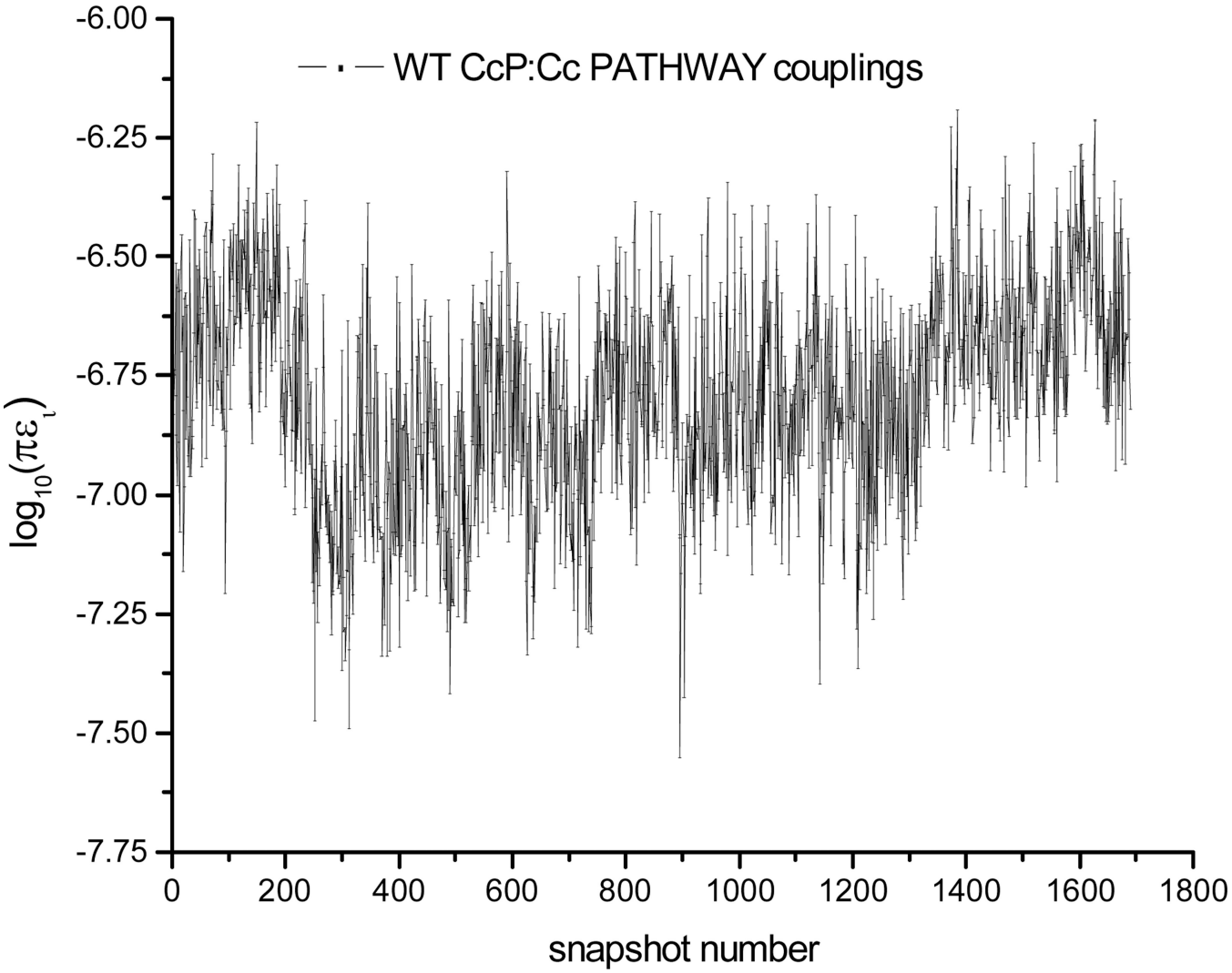

Figure 5.
Logarithm of PATHWAY coupling versus snapshot number for the WT CcP:Cc complex. The time step between snapshots is 2 ps.

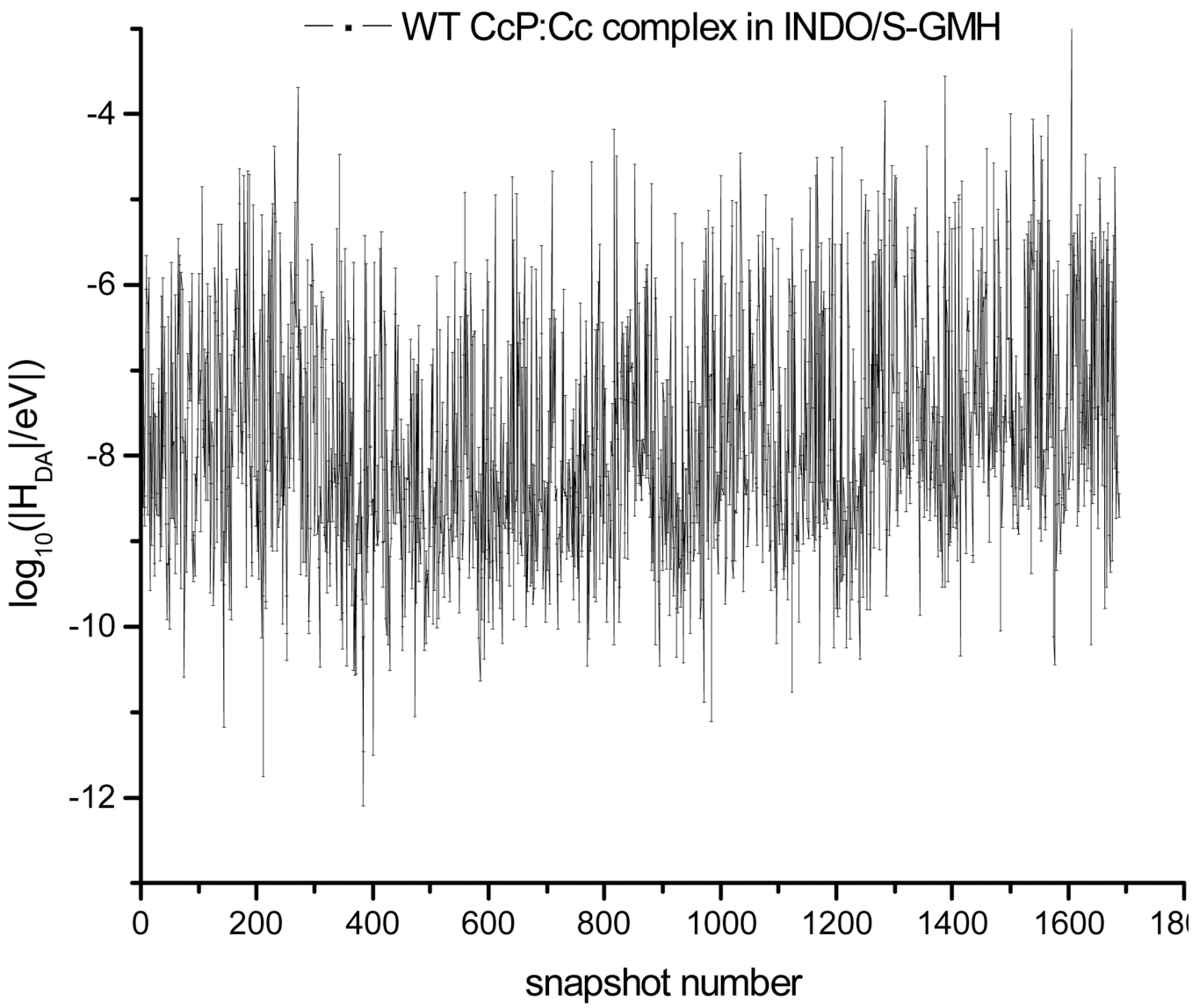

Figure 6.
Logarithm of $|H_{DA}|$ versus snapshot number for the WT CcP:Cc complex from INDO-GMH calculations. The time step between snapshots is 2 ps.

Table 1

Measured back ET rate constants for the fast kinetic phase in solution and in crystals, and donor-acceptor distances from crystal structures. The relative mean-squared electronic couplings from the PATHWAY model with respect to the WT values appear in the last column. $\langle H_{DA}^2 \rangle_{rel} = \langle H_{DA}^2 \rangle / \langle H_{DA}^2 \rangle^{WT}$ based on Fe-to-ZnP tunneling.

	Crystal Data [a]		Soln Data[b]	PW[c]		
	k_{eb} (s^{-1})	R_{Zn-Fe} (Å)	R_{ed-ed} (Å)	$R_{trp-heme}$ (Å)	k_{eb} (s^{-1})	$\langle H^2_{DA} \rangle_{rel}$
WT	6,000	26.5	15.6	13.6	4,900	1
F82W	5,800	26.4	15.6	14.0	--	1.0
F82S	2,000	26.3	15.4	13.5	2,500	1.0
F82I	2,100	29.8	22.6	19.4	1,900	0.02
F82Y	4,000	29.4	22.8	19.6	4,300	0.003

[a] All taken from Ref. 7.

[b] All are taken from Ref. 17.

[c] Heme-ZnP PATHWAY couplings

Table 2

Calculated mean-squared ET couplings based on INDO-GMH analysis for six protein complexes with and without Trp191 as the acceptor.

	With Trp191	Without Trp191
	$\langle H_{DA}^2 \rangle 10^{-14} eV^2$	$\langle H_{DA}^2 \rangle 10^{-14} eV^2$
WT	4,700	7.7
F82W	8,300	11
F82S	5,800	6.2
F82I	6.8	0.15
F82Y	8.6	0.41
W191F	--	3.9

Table 3

Computed reorganization energies and associated rates for the WT CcP:Cc complex and four mutants. (ε_{op} = 2, $\varepsilon_s^{protein}=4$, and $\varepsilon_s^{solvent}=80$); ε_S = 4 in the Marcus model).

	$\langle H_{DA}^2\rangle$ (10^{-14}eV^2) total	$\langle H_{DA}^2\rangle$ (10^{-14}eV^2) heme-ZnP	λ (*FDPB*;2S) (eV)	E(Fe^{II}Cc/Fe^{III}Cc) (V)	Δ*G* (eV)	$b_e^{-(\Delta G+\lambda)^2/4\lambda kT}$	$c_{k_{max}}$ (sec^{-1}) total	$c_{k_{max}}$ (sec^{-1}) heme-ZnP
WT	4.7×10^3	7.7	0.60; 0.74	0.234	−0.97	0.1	1.0×10^6	1.6×10^3
F82W	5.8×10^3	6.2	0.64; 0.74	0.251	−0.95	0.22	1.2×10^6	1.2×10^3
F82S	8.3×10^3	11	0.50; 0.73	0.188	−1.01	0.076	2.0×10^6	2.6×10^3
F82I	6.8	0.15	1.07; 0.83	0.216	−0.98	0.93	1.1×10^3	2.4×10^1
F82Y	8.6	0.41	1.05; 0.83	0.206	−0.99	0.96	1.4×10^3	6.7×10^1
W191F	-	3.9	0.90; --	-	−1.13			7.0×10^2

[a] Values are calculated using E(Fe^{II}Cc/Fe^{III}Cc) mutants from Ref. 115). and E(ZnCcP$^+$/Zn CcP) =1.20 V (Ref 116).

[b] All values for FDPB values of λ.

[c] $k_{max}=(2\pi/\hbar)\langle H_{DA}^2\rangle/\sqrt{4\pi\lambda^{FDPB}kT}$

2S = two-sphere; FDPB = finite-difference Poisson-Boltzmann.

J Phys Chem B. Author manuscript; available in PMC 2014 August 08.

Table 4

Computed fast- and slow-phase back ET rate constants for the WT and mutant CcP:Cc complexes. The rate constants were computed using the experimental Δ G values[1] and λ values from FDPB calculations ($k_{max} \times e^{-(\Delta G+\lambda)^2/4\lambda kT}$ from Table 3).

	k_{eb1}^{calc} s^{-1}	k_{eb2}^{calc} s^{-1}	$^{a}k_{eb1}^{exp}$ s^{-1}	$^{a}k_{eb2}^{exp}$ s^{-1}
WT	1×10^5	200	6000[b]	--
F82W	2×10^5	300	5800	60
F82S	1×10^5	200	2000	70
F82I	1000	20	4000	70
F82Y	1000	60	2100	40
W191F	--	400	--	74

[a] Experimental k_{eb} values taken from Ref. 7; calculated k_{eb} values are obtained using the ΔG values of Table 3.

[b] Lower bound.

(1) Rafferty, S. P.; Pearce, L. L.; Barker, P. D.; Guillemette, J. G.; Kay, C. M.; Smith, M.; Mauk, A. G. Electrochemical, Kinetic, and Circular Dichroic Consequences of Mutations at Position 82 of Yeast Iso-1-Cytochrome C. *Biochemistry* **1990**, *29*, 9365–9369.